Gradient-based Magnetic Resonance Electrical Properties Imaging of Brain Tissues

Jiaen Liu *Student Member, IEEE*, Xiaotong Zhang, *Member, IEEE*, Sebastian Schmitter, Pierre-Francois Van de Moortele and Bin He, *Fellow, IEEE*

***Abstract*— Electrical properties tomography (EPT) holds promise for noninvasively mapping at high spatial resolution the electrical conductivity and permittivity of biological tissues *in vivo* using a magnetic resonance imaging (MRI) scanner. In the present study, we have developed a novel gradient-based EPT approach with greatly improved tissue boundary reconstruction and largely elevated robustness against measurement noise compared to existing techniques. Using a 7 Tesla MRI system, we report, for the first time, high-quality *in vivo* human brain electrical property images with refined structural details, which can potentially merit clinical diagnosis (such as cancer detection) and high-field MRI applications (quantification of local specific absorption rate) in the future.**

I. Introduction

The frequency-dependent electrical properties (EPs), which consist of the conductivity and the permittivity, largely vary as a function of the relative intracellular and extracellular fluid volumes, ionic concentrations and the cellular membrane extent in the biological tissues [1]. The conductivity and permittivity can be affected by various pathological conditions, such as cancers, ischemia, hemorrhage and edema, etc. Therefore, it is anticipated that imaging electrical properties may provide important information to diagnose and monitor the progression of a variety of diseases.

In the past three decades, substantial research efforts have been made on multiple fronts with the goal of non-invasively mapping EPs of biological tissues. Electrical Impedance Tomography (EIT) inversely reconstructs impedance images from electric potential measurement induced by current injection through surface electrodes [2], [3], while its major limitation lies in its poor spatial resolution due to a limited amount of measured data and the ill-posedness of the corresponding inverse reconstruction problem. Magnetic Resonance Electrical Impedance Tomography (MREIT), which originates from Magnetic Resonance Current Density Imaging (MRCDI) [4], measures the local magnetic field induced by surface current injection, and reconstructs static cross-sectional conductivity images [5]–[7]; however, this approach is still facing unsolved safety issues due to the necessary usage of high level of current injection in order to achieve sufficient signal-to-noise ratio (SNR). Magneto-acoustic Tomography with Magnetic Induction (MAT-MI) exploits the Lorentz force effect of the interaction between a magnetic field and eddy current induced by a time varying magnetic field to emit acoustic signals for conductivity image reconstruction [8]–[10]; but besides focusing on gel phantoms and tissue samples, there have been no *in vivo* experiments reported so far.

MR based Electrical Properties Tomography (EPT) utilizes measurable radiofrequency-coil-induced magnetic fields (B_1 fields) in an MRI system to quantitatively and noninvasively reconstruct the local *in vivo* EPs of biological tissues. The concept of imaging EPs from MR signals was firstly suggested by Haacke et al. [11] and Wen [12]. In recent years, EPT has drawn considerable attention by various research groups. Based upon well-established B_1-mapping techniques in MRI, various EPT methods have been proposed using different coil designs (e.g. birdcage quadrature, multi-channel array coil) and at different radiofrequencies (64MHz~300MHz) corresponding to the operating static main field (1.5T~7T) [13]–[19].

In the meantime, unlike other EPs imaging modalities, EPT reconstructs EPs at the operating Larmor frequency of MRI. The local EPs values provide important information in quantifying local Specific Absorption Rate (SAR) [20], which is a major safety concern in high-field (HF: 3 Tesla and above) MRI. Knowing EPs distribution can help deduce radiofrequency (RF) electric fields, allowing for fast and subject-specific SAR estimation, which can serve as a constrain of MRI pulse design to achieve more effective and safer RF excitation in HF- and UHF-MRI applications.

Biological tissues may exhibit rapid spatial changes in electrical properties due to small size of tissue. Such scenario has been a challenge to existing EPT approaches as most of them are based upon formulations assuming locally homogeneous EPs [13]–[16], leading to significant errors in the vicinity of tissue boundaries in reconstructed EPs maps [21]. Another major challenge results from the involved Laplacian operation over B_1 field during reconstruction, making the calculation sensitive to noise in the measured B_1 maps. Due to necessary spatial filters with relatively large kernel to smooth the B_1 data, effective spatial resolution can be decreased, and significant distortions inevitably occur near boundaries in the reconstructed EPs maps [21].

In this study, a novel gradient-based EPT approach (named as gEPT algorithm) is proposed, in which the spatial gradients

This work was supported in part by NIH RO1EB006433, RO1EB007920, R21EB017069, R21EB009133, R21EB014353, P41RR008079, P30NS057091, and U01HL117664.

J. Liu is with the Department of Biomedical Engineering, University of Minnesota, Minneapolis, MN 55455, USA.
X. Zhang is with the Department of Biomedical Engineering, University of Minnesota, Minneapolis, MN 55455, USA.
S. Schmitter is with the Center for Magnetic Resonance Research, University of Minnesota, Minneapolis, MN 55455, USA.
P.-F. Van de Moortele is with the Center for Magnetic Resonance Research, University of Minnesota, Minneapolis, MN 55455, USA.
B. He is with the Department of Biomedical Engineering and Institute for Engineering in Medicine, University of Minnesota, Minneapolis, MN 55455, USA.

978-1-4244-7929-0/14/$26.00 ©2014 IEEE

of the electrical properties are explicitly considered in the algorithm, and utilized to reconstruct EPs maps through spatial integration. Through a series of simulation study, phantom validation and *in vivo* experiments at 7T, the reported approach is capable of reconstructing EPs maps with highly refined structural details and improved robustness against noise contamination.

II. Gradient-based EPT Algorithm

Consider the magnetic permeability inside the biological tissues to be equal to that in the vacuum. In their time-harmonic form, Faraday's and Ampere's Laws can be combined to obtain

$$-\nabla^2\mathbf{H} = \omega^2\mu_0\varepsilon_c\mathbf{H} + (\nabla\varepsilon_c/\varepsilon_c)\times(\nabla\times\mathbf{H}) \qquad (1)$$

where $\mathbf{H}$ is the RF-coil-induced magnetic field strength vector in the Cartesian coordinate, ω the operating angular frequency (Larmor frequency), $\varepsilon_c = \varepsilon - i\sigma/\omega$ the complex permittivity as a function of the electrical conductivity σ and the permittivity ε, ε_0 and μ_0 are the free space permittivity and permeability, respectively. Although distribution of the Cartesian components of the RF magnetic fields cannot be measured straightforwardly in MRI, the principle of reciprocity [22] links transverse RF magnetic field components in Cartesian and rotating frames. Therefore, the EPT problem lies in the course that: simplified Eq. (1) is re-formalized into B_1 terms in the rotating frames, i.e. H_1^+ and/or H_1^-. Within RF coils such as birdcage and transverse electromagnetic (TEM) microstrip coils, the H_z component of H can be ignored [14], [23], and Eq. (1) can be transformed into the form of H_1^+ and/or H_1^- as

$$\begin{cases} \nabla^2 H_1^+ = -\omega^2\mu_0 H_1^+\varepsilon_c + \nabla H_1^+ \cdot \begin{bmatrix} 1 & i & 0 \\ -i & 1 & 0 \\ 0 & 0 & 1 \end{bmatrix} \cdot \nabla \ln \varepsilon_c \\ \nabla^2 H_1^- = -\omega^2\mu_0 H_1^-\varepsilon_c + \nabla H_1^- \cdot \begin{bmatrix} 1 & -i & 0 \\ i & 1 & 0 \\ 0 & 0 & 1 \end{bmatrix} \cdot \nabla \ln \varepsilon_c \end{cases} \qquad (2)$$

Eq. (2) is the central equation of gEPT algorithm. It can be further decomposed into variables including 1) known (measurable) variables such as B_1 magnitude and *relative* phase of individual RF channels, 2) unknown variables such as ε_c, $\nabla \ln \varepsilon_c$, as well as *absolute* B_1 phase. Utilizing measured B_1 data sets from multiple RF channels, a set of equations can be formed to derive the gradient $\nabla \ln \varepsilon_c$. Then using predetermined value of electrical properties at one (or several) seed location(s), quantitative maps of ε_c can be determined from the gradient using the finite-difference method in the imaging plane [24]. Taking advantage of derived $\nabla \ln \varepsilon_c$, reduced boundary artifact and improved robustness against noise contamination are anticipated to improve the overall reconstruction performance.

III. Methods

A. Simulation Evaluation

Electromagnetic simulation was performed based on the finite-difference time-domain (FDTD) method in software SEMCAD (Schmid & Partner Engineering AG, Zurich, Swizerland). A 16-channel microstrip array coil [25], which was used in the experimental part of the study, was numerically modeled and loaded with either the Duke head model of the Virtual Family [26] (Fig. 1(a)) or a homogeneous cylindrical model (Fig. 1(b)) whose diameter was 15 cm, height 20 cm, σ 0.55 Sm^{-1} and ε 52 ε_0. For each coil element, the complex magnetic field at the frequency of 298 MHz (Larmor frequency of proton at 7 T) was simulated with a voxel size of 2×2×2 mm^3.

B. Experiment Setting

Experiments were carried out on a 7 T whole body MRI scanner (Siemens, Erlangen, Germany). A 16-channel microstrip array RF coil [25] was utilized for all experiments, powered by 16×1kW amplifiers (CPC, Hauppauge, NY, USA) controlled by a remotely operated 16-channel RF phase/amplitude gain unit. By employing a hybrid B_1-mapping technique (merging large and small flip angle data for B_1 mapping) [27]–[31], magnitude of H_1^+ and H_1^- for individual channel, as well as their *relative* phase maps between each channel can be acquired for the subsequent calculations of EPs.

A two-compartment 3D phantom, made by a plastic jar with a plastic bottle positioned in the center, was filled with saline gel solutions consisting of different concentrations of distilled water, NaCl, Sucrose, $CuSO_4 \cdot 5H_2O$ and gelatin. The electrical properties of inner and outer solutions were σ=0.34 S m^{-1} / ε=77 ε_0 and σ=0.12 S m^{-1} / ε=78 ε_0, respectively, as measured with an Agilent 85070E dielectric probe kit and an Agilent E5061B network analyzer (Agilent, Santa Clara, CA, USA). The phantom was positioned at the isocenter of the RF coil. B_1 data was acquired with a spatial resolution of 1.5×1.5×3 mm^3. The electrical properties on its central transverse slice were reconstructed using the proposed gEPT approach with the central point as the seed point.

One healthy human subject, who signed consent form approved by the Institutional Review Board at the University of Minnesota, was scanned in the supine position with the head centered in the same RF coil as in the phantom experiment. A spatial resolution of 1.5×1.5×5 mm^3 was utilized for B_1 data acquisition. The proposed gEPT algorithm was used to generate EPs maps in the brain *in vivo*.

IV. Results

Fig. 1(a) exhibits the results of reconstructed σ and ε in a transverse slice using the proposed gEPT under noise-free condition, with six seed points indicated by the symbol 'o'. In general, it can be seen in Fig. 1(a) that the detailed structural information present in the target maps was accurately reproduced in the reconstructed maps of σ and ε using gEPT;

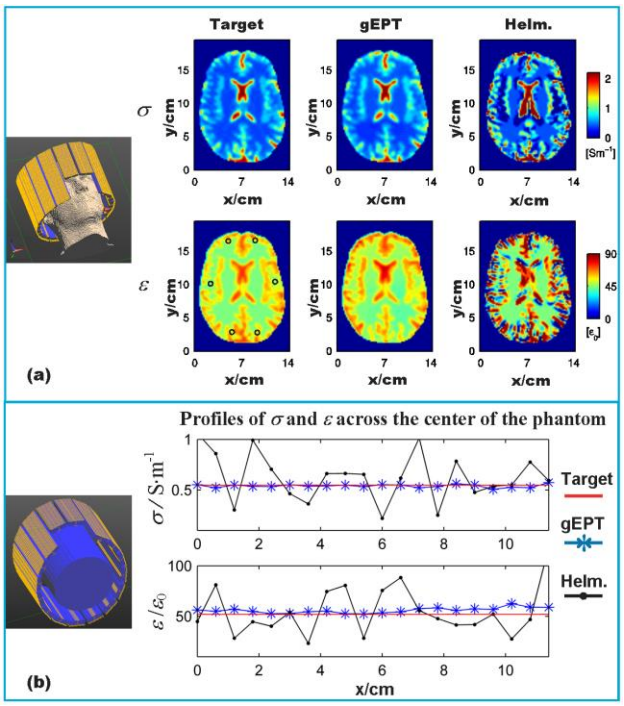

Figure. 1 (a) The reconstructed electrical properties of the Duke head model based on gEPT and homogeneous Helmholtz equation with respective to the target images, respectively, under noise-free condition. 'o': location of seed points (b): Profiles of target and reconstructed electrical properties of the homogeneous phantom model under noise condition (SNR=50).

the relative error (RE) and correlation coefficient (CC) of the reconstruction are *RE*=8.5% / *CC*=0.98 for σ reconstruction, and *RE*=7.6% / *CC*=0.90 for ε reconstruction, respectively. In contrast, using the homogeneous Helmholtz equation in classic EPT methods [13], [15], substantial distortion was induced near the boundaries separating different tissues as shown in Fig. 1(a), with *RE*=99.7% / *CC*=0.38 for σ reconstruction and *RE*=58.0% / *CC*=0.25 for ε reconstruction, respectively.

In Fig 1(b), we compared the results using gEPT and Helmholtz equation in the homogeneous phantom model. Random white noise whose standard deviation was 1/50 of the magnitude of B_1 field was added to the simulated B_1 data. The noise contaminated data was smoothed with a Gaussian filter of size 3 pixels and sigma 0.8 pixels. On the same smoothed B_1 data set, gEPT and Helmholtz-based approach were carried out individually. As can be seen, the results using gEPT (RE_σ= 10.0% and RE_ε=13.6%) were much closer to the target than that derived from the Helmholtz-based approach (RE_σ= 90.7% and RE_ε=62.0%) even if the phantom's electrical properties were homogeneous.

The reconstructed EPs maps for the central transverse slice are shown in Fig. 2(b). In general, the reconstructed results showed conspicuous agreement with probe-measured values. In the central compartment, the reconstructed σ is 0.30±0.05 Sm^{-1} (mean ± standard deviation) and ε is 74±3 ε_0; in the periphery, the reconstructed σ is 0.12±0.05 Sm^{-1} and ε is 73±3 ε_0. Due to the absence of visible MR signal in plastic materials

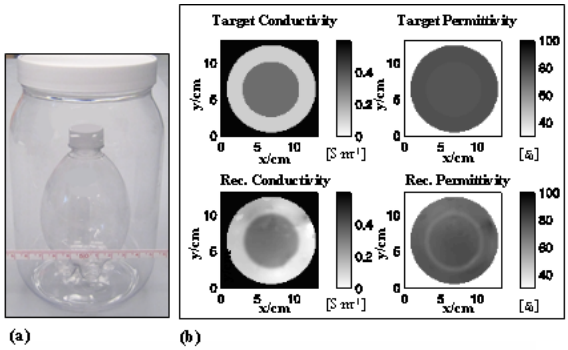

Figure. 2 (a) Photograph of the phantom container to be filled with gel solutions. (b) The reconstructed electrical properties using gEPT in a transverse slice.

(very short T_2) at the standard echo times utilized in our sequences, some artifacts are observed in the reconstructed permittivity map near the thin plastic wall between the center and periphery of the phantom.

Fig. 3 shows, on the slice of interest, estimated electrical properties of brain tissues of the subject. With respect to the corresponding T_1 structural images, the estimated electrical property distributions demonstrate strong similarity to the anatomical structures. The estimated results for gray matter (GM), white matter (WM) and cerebrospinal fluid (CSF) are σ_{GM}=0.61±0.15 Sm^{-1}, σ_{WM}=0.52±0.10 Sm^{-1} and

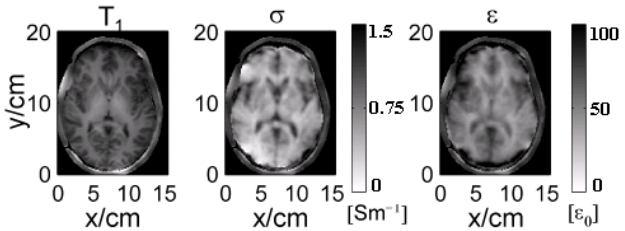

Figure. 3 Reconstructed electrical properties in the transverse slices in the brain of the human subject in comparison with the T_1-weighted image.

σ_{CSF}=1.24±0.11 Sm^{-1}; ε_{GM}=57.3±9.7 ε_0, ε_{WM}=47.6±5.9 ε_0 and ε_{CSF}=71.1±7.3 ε_0. Here, literature reported values [1] of σ_{GM}=0.69 Sm^{-1}, σ_{WM}=0.43 Sm^{-1} and σ_{CSF}=2.2 Sm^{-1}; ε_{GM}=60.1 ε_0, ε_{WM}=43.8 ε_0 and ε_{CSF}=72.8 ε_0 were quoted as a reference. Near the periphery of the brain, i.e. in the vicinity of the skull, larger errors are observed, which can arise from the almost complete absence of MR signal in bones.

V. Discussion

In this study, we have proposed a novel method – gradient-based Electrical Properties Tomography (gEPT) – for *in vivo* imaging of electrical properties using MRI, and demonstrated, for the first time, high quality *in vivo* human brain EPT imaging. This approach is characterized by two advantages overcoming the aforementioned challenges in current EPT development. First of all, the gradient term in Eq. (2) provides necessary information for accurate reconstruction along the boundaries of tissues with different electrical properties. Secondly, because spatial integration was used to obtain the map of electrical properties, it was demonstrated that the result becomes more robust to noise and

calculation errors in comparison with the classic non-gradient-based electrical properties estimation. It was noticed that *a priori* EPs information at certain seed points is needed to transfer the estimated gradient into absolute EPs maps. We have investigated in simulation studies that the performance is insensitive to the selection of different seed points. For future *in vivo* application, this information can be more robustly obtained from regions with relatively uniform EPs distribution that can be identified by other image methods, e.g., structural MRI, in which other EPT methods can be exploited to obtain the local EPs values with eliminated sensitivity to boundary effect. On the other hand, the estimated relative EPs maps can potentially provide useful diagnostic information as a local contrast mechanism.

Based on the proposed gEPT approach, our *in vivo* study at 7T exhibited electrical-property images of the human brain with clearly identified anatomical structures, such as gray/white matter and ventricles, consistent with the same structures identified in T_1 contrast image of the same slice. Based on its demonstrated tissue-contrast properties, it is anticipated that the proposed method may significantly impact clinical applications in the future.

REFERENCES

[1] S. Gabriel, R. W. Lau, and C. Gabriel, "The dielectric properties of biological tissues: II. Measurements in the frequency range 10 Hz to 20 GHz," *Phys. Med. Biol.*, vol. 41, no. 11, pp. 2251–2269, Nov. 1996.

[2] P. Metherall, D. C. Barber, R. H. Smallwood, and B. H. Brown, "Three-dimensional electrical impedance tomography," *Nature*, vol. 380, no. 6574, pp. 509–512, 1996.

[3] J. L. Mueller, D. Isaacson, and J. C. Newell, "A reconstruction algorithm for electrical impedance tomography data collected on rectangular electrode arrays," *Biomed. Eng. IEEE Trans.*, vol. 46, no. 11, pp. 1379–1386, Nov. 1999.

[4] M. Joy, G. Scott, and M. Henkelman, "In vivo detection of applied electric currents by magnetic resonance imaging," *Magn. Reson. Imaging*, vol. 7, no. 1, pp. 89–94, 1989.

[5] N. Zhang, "Electrical Impedance Tomography Based on Current Density Imaging," M.S. thesis, Univ. Toronto, Toronto, ON, Canada, 1992.

[6] O. Kwon, E. J. Woo, J.-R. Yoon, and J. K. Seo, "Magnetic resonance electrical impedance tomography (MREIT): simulation study of J-substitution algorithm," *IEEE Trans. Biomed. Eng.*, vol. 49, no. 2, pp. 160–167, Feb. 2002.

[7] N. Gao and B. He, "Noninvasive Imaging of Bioimpedance Distribution by Means of Current Reconstruction Magnetic Resonance Electrical Impedance Tomography," *IEEE Trans. Biomed. Eng.*, vol. 55, no. 5, pp. 1530–1538, 2008.

[8] Y. Xu and B. He, "Magnetoacoustic tomography with magnetic induction (MAT-MI)," *Phys. Med. Biol.*, vol. 50, no. 21, pp. 5175–5187, Nov. 2005.

[9] X. Li and B. He, "Multi-excitation magnetoacoustic tomography with magnetic induction for bioimpedance imaging," *IEEE Trans. Med. Imaging*, vol. 29, no. 10, pp. 1759–1767, Oct. 2010.

[10] L. Mariappan and B. He, "Magnetoacoustic Tomography with Magnetic Induction: Bioimepedance reconstruction through vector source imaging," *IEEE Trans. Med. Imaging*, Jan. 2013.

[11] E. M. Haacke, L. S. Petropoulos, E. W. Nilges, and D. H. Wu, "Extraction of conductivity and permittivity using magnetic resonance imaging," *Phys. Med. Biol.*, vol. 36, no. 6, pp. 723–734, Jun. 1991.

[12] H. Wen, "Noninvasive quantitative mapping of conductivity and dielectric distributions using RF wave propagation effects in high-field MRI," San Diego, CA, USA, 2003, vol. 5030, pp. 471–477.

[13] U. Katscher, T. Voigt, C. Findeklee, P. Vernickel, K. Nehrke, and O. Dossel, "Determination of Electric Conductivity and Local SAR Via B1 Mapping," *Med. Imaging IEEE Trans.*, vol. 28, no. 9, pp. 1365–1374, Sep. 2009.

[14] T. Voigt, U. Katscher, and O. Doessel, "Quantitative conductivity and permittivity imaging of the human brain using electric properties tomography," *Magn. Reson. Med.*, vol. 66, no. 2, pp. 456–466, 2011.

[15] A. L. van Lier, D. O. Brunner, K. P. Pruessmann, D. W. J. Klomp, P. R. Luijten, J. J. W. Lagendijk, and C. A. T. van den Berg, "B 1+ Phase mapping at 7 T and its application for in vivo electrical conductivity mapping," *Magn. Reson. Med.*, vol. 67, no. 2, pp. 552–561, 2012.

[16] U. Katscher, C. Findeklee, and T. Voigt, "B1-based specific energy absorption rate determination for nonquadrature radiofrequency excitation," *Magn. Reson. Med.*, vol. 68, no. 6, pp. 1911–1918, 2012.

[17] X. Zhang, P.-F. V. de Moortele, S. Schmitter, and B. He, "Complex B1 mapping and electrical properties imaging of the human brain using a 16-channel transceiver coil at 7T," *Magn. Reson. Med.*, vol. 69, no. 5, pp. 1285–1296, 2013.

[18] X. Zhang, S. Schmitter, P. Van de Moortele, J. Liu, and B. He, "From Complex B1 Mapping to Local SAR Estimation for Human Brain MR Imaging Using Multi-Channel Transceiver Coil at 7T," *IEEE Trans. Med. Imaging*, vol. 32, no. 6, pp. 1058–1067, 2013.

[19] J. Liu, X. Zhang, P.-F. Van de Moortele, S. Schmitter, and B. He, "Determining electrical properties based on B(1) fields measured in an MR scanner using a multi-channel transmit/receive coil: a general approach," *Phys. Med. Biol.*, vol. 58, no. 13, pp. 4395–4408, Jul. 2013.

[20] C. M. Collins, W. Liu, J. Wang, R. Gruetter, J. T. Vaughan, K. Ugurbil, and M. B. Smith, "Temperature and SAR calculations for a human head within volume and surface coils at 64 and 300 MHz," *J. Magn. Reson. Imaging JMRI*, vol. 19, no. 5, pp. 650–656, May 2004.

[21] J. K. Seo, M.-O. Kim, J. Lee, N. Choi, E. J. Woo, H. J. Kim, O. I. Kwon, and D.-H. Kim, "Error analysis of nonconstant admittivity for MR-based electric property imaging," *IEEE Trans. Med. Imaging*, vol. 31, no. 2, pp. 430–437, Feb. 2012.

[22] D. I. Hoult, "The principle of reciprocity in signal strength calculations—A mathematical guide," *Concepts Magn. Reson.*, vol. 12, no. 4, pp. 173–187, Jan. 2000.

[23] X. Zhang, S. Zhu, and B. He, "Imaging Electric Properties of Biological Tissues by RF Field Mapping in MRI," *IEEE Trans. Med. Imaging*, vol. 29, no. 2, pp. 474–481, Feb. 2010.

[24] A. Iserles, *A First Course in the Numerical Analysis of Differential Equations*. Cambridge University Press, 2009.

[25] G. Adriany, P.-F. Van de Moortele, J. Ritter, S. Moeller, E. J. Auerbach, C. Akgün, C. J. Snyder, T. Vaughan, and K. Uğurbil, "A geometrically adjustable 16-channel transmit/receive transmission line array for improved RF efficiency and parallel imaging performance at 7 Tesla," *Magn. Reson. Med.*, vol. 59, no. 3, pp. 590–597, Mar. 2008.

[26] A. Christ, W. Kainz, E. G. Hahn, K. Honegger, M. Zefferer, E. Neufeld, W. Rascher, R. Janka, W. Bautz, J. Chen, B. Kiefer, P. Schmitt, H.-P. Hollenbach, J. Shen, M. Oberle, D. Szczerba, A. Kam, J. W. Guag, and N. Kuster, "The Virtual Family—development of surface-based anatomical models of two adults and two children for dosimetric simulations," *Phys. Med. Biol.*, vol. 55, no. 2, p. N23, Jan. 2010.

[27] V. L. Yarnykh, "Actual flip-angle imaging in the pulsed steady state: A method for rapid three-dimensional mapping of the transmitted radiofrequency field," *Magn. Reson. Med.*, vol. 57, no. 1, pp. 192–200, Jan. 2007.

[28] P.-F. Van de Moortele, C. Akgun, G. Adriany, S. Moeller, J. Ritter, C. M. Collins, M. B. Smith, J. T. Vaughan, and K. Uğurbil, "B1 destructive interferences and spatial phase patterns at 7 T with a head transceiver array coil," *Magn. Reson. Med.*, vol. 54, no. 6, pp. 1503–1518, Dec. 2005.

[29] P.-F. Van de Moortele, C. Snyder, L. DelaBarre, G. Adriany, T. Vaughan, and K. Ugurbil, "Calibration Tools for RF Shim at Very High Field with Multiple Element RF Coils: from Ultra Fast Local Relative Phase to Absolute Magnitude B1+ Mapping," presented at the Proc. of ISMRM, Berlin, Germany, 2007, p. 1676.

[30] P.-F. Van de Moortele and K. Uğurbil, "Very Fast Multi Channel B1 Calibration at High Field in the Small Flip Angle Regime," presented at the Proc. of ISMRM, Hawaii, USA, 2009, p. 367.

[31] D. O. Brunner and K. P. Pruessmann, "B 1+ interferometry for the calibration of RF transmitter arrays," *Magn. Reson. Med.*, vol. 61, no. 6, pp. 1480–1488, 2009.